JOURNAL OF MATERIALS SCIENCE 7 (1972) 115–123

Amplitude-Independent Mechanical Damping in Alkali Halides

W. H. ROBINSON
Physics and Engineering Laboratory, Department of Scientific and Industrial Research, Wellington, New Zealand

At present there are two theories which are used to explain the observed amplitude-independent mechanical damping (internal friction) in alkali halides. In the theory of Granato and Lücke it is assumed that the damping constant, B, results from the dislocation interacting with phonons, while in the theory of Robinson and Birnbaum, the assumption is made that the dislocation drag is caused by charged dislocations, interacting with their compensating charge clouds. Both these theories predict a peak in the damping at a frequency of ~ 10 MHz but the peak in the R-B theory is far less sharp than that in the G-L theory.

In this paper the MHz results of Suzuki, Ikushima, and Aoki for room temperature and the MHz results of Mitchell taken at 77 and 298 K are, together with some kHz results, compared with the two theories. It is shown that both the theories are able to explain the effect of temperature and irradiation but that the theory of Granato and Lücke does not fit the kHz results as well as the theory of Robinson and Birnbaum. The phonon damping analysis gives a change in B of a factor of 14 between the LiF specimens of Suzuki *et al* and Mitchell while for the charge cloud analysis the charges on the dislocations within the LiF specimen differ only by 20%.

It is concluded that the charge cloud damping theory with a damping constant as a function of frequency fits the experimental results better than the present phonon damping theory which has a damping constant not dependent on frequency.

1. Introduction

When a stress is applied to a crystalline material the dislocations within the crystals will tend to move though their motion will be resisted by pinning points (e.g. impurities) and by a viscous drag force. The viscous drag force will play an important role in the behaviour of the material when it is deformed, since on deformation the dislocations break away from their pinning points and move rapidly over large distances. The measured plastic strain is the sum of the motion of all these dislocations. The distance they move, and therefore the plastic strain, is strongly dependent on the drag force resisting their motion. In alkali halides the drag force can be determined from the mechanical damping (internal friction) as the main contribution to the damping is due to the motion of dislocations [1-4]. When they are forced to oscillate by an applied stress, these dislocations can be thought of as vibrating strings oscillating within a viscous medium and thereby absorbing acoustic energy. The mechanical damping parameter, ϕ or Q^{-1}, defined as the energy lost per cycle of vibration divided by 2π times the total energy of vibration, is a measure of the viscous drag acting on the dislocations.

In their theory, originally developed for amplitude-independent damping in metals, Granato and Lücke [5] assume that this viscous damping is due to the interaction of the moving dislocations with phonons (thermal vibrations). Leibfried [6] and Mason [7] have separately arrived at expressions for the damping constant which are not dependent on the frequency at which the dislocation is oscillating. The theory of Granato and Lücke with a frequency independent damping constant has been applied to the dislocation damping of alkali halides with some success [8].

To explain the observed amplitude-independent damping in ionic crystals at high temperatures, Robinson and Birnbaum have developed another theory [3]. This is based on the fact that in ionic solids, dislocations can carry electrical charges in the form of jogs [9], and that these charged dislocations are surrounded by charge clouds formed by cation vacancies, anion vacancies, and divalent impurities, with a slight excess of point defects of one sign to compensate for the charge on the dislocation. When the charged dislocations are moved from the centre of their charge clouds, the charge clouds are pulled after them by the coulomb force. The drag force which is frequency dependent, has components which contribute to the mechanical damping and to the compliance defect (modulus defect). This theory of Robinson and Birnbaum has been used to explain the observed mechanical damping in alkali halides at room temperature [10].

The main differences between the theories of Granato and Lücke (G-L) and Robinson and Birnbaum (R-B) are the shapes of the damping and compliance defect versus frequency curves (figs. 1 and 2). At low frequencies ϕ (G-L) is proportional to frequency while ϕ (R-B) is proportional to the logarithm of frequency. The compliance defect in the G-L case has a maximum at low frequencies, remains constant until just before ω (max) where it starts to fall to zero, while in the R-B theory it has a maximum at a frequency just below ω (max) and minimum at a frequency just above ω (max) and varies continuously with frequency. The theory of Robinson and Birnbaum also predicts a maximum in damping at iso-electric temperatures where the charge on the dislocation goes to zero. Another difference of importance is the effect of irradiation on the damping constant B. If on irradiation the concentration of charged point defects or the charge on the dislocation increases, then in the theory of Robinson and Birnbaum the damping constant will increase, while for the Granato and Lücke theory it is invariant.

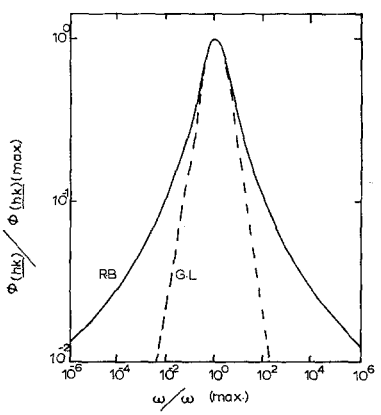

Figure 1 Normalised plots of Mechanical Damping versus Radial Frequency. The solid line is
$\phi(\underline{hk})/\phi(\underline{hk})(\max) = \{4[\ln\omega/\omega(\max)]^2/\pi^2 + 1\}^{-1}$
(charge cloud theory) and the dashed one
$\phi(\underline{hk})/\phi(\underline{hk})(\max) = 2[\omega/\omega(\max)]/[1 + (\omega/\omega(\max))^2]$
(phonon theory).

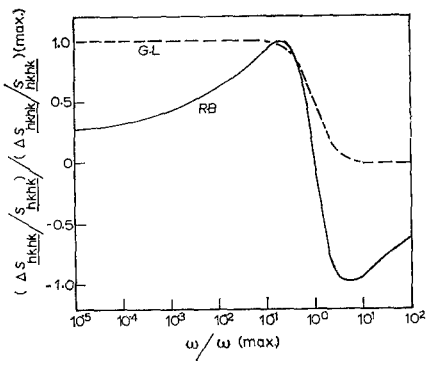

Figure 2 Normalised plots of Compliance Defect versus Radial Frequency. The solid line is
$(\Delta S_{\underline{hkhk}}/S_{\underline{hkkk}})/(\Delta S_{\underline{hkhk}}/S_{\underline{hkhk}})(\max) = -4\ln\omega/\omega(\max)/\{4[\ln\omega/\omega(\max)]^2/\pi^2 + 1\}\,\pi$
(charge cloud theory) and the dashed one
$(\Delta S_{\underline{hkhk}}/S_{\underline{hkhk}})/(\Delta S_{\underline{hkhk}}/S_{\underline{hkhk}})(\max) = [1 + (\omega/\omega(\max))^2]^{-1}$
(phonon theory).

2. Theory

Consider the forces per unit length, acting on a dislocation of loop length l between pinning points (point defects and dislocation nodes), forced to vibrate with a radial frequency ω, by an applied stress $\sigma_{mn} \sin \omega t$. For longitudinal waves $\sigma_{mn} = \sigma_{11}$ while for shear waves $\sigma_{mn} = \sigma_{12} = \sigma_{21}$. If ξ_w is the component of the displacement of the dislocation in its slip plane in direction w at a point y along its length, then the equation which needs to be satisfied for the equilibrium of forces acting on the dislocation is

$$A\frac{\partial^2\xi_w}{\partial t^2} + B\frac{\partial\xi_w}{\partial t} - C\frac{\partial^2\xi_w}{\partial y^2} = a_{wmn}\,\sigma_{mn}\sin\omega t \qquad \ldots\ldots (1)$$

with the boundary conditions

$$\xi_w(0, t) = \xi_w(l, t) = 0$$

(dislocation fixed at pinning points or dislocation nodes).

$A\,(\partial^2\xi_w/\partial t^2)$ is the force due to the inertia of the dislocation, A being the effective mass per unit length of the dislocation. $A \approx \rho\,\pi\,b^2$ where ρ is the density of the material and b the magnitude of Burgers vector.

$B\,(\partial\xi_w/\partial t)$ is the viscous term; in metals B is due to phonon drag and is not frequency dependent [5-7]. In the charged dislocation theory [3, 11], B is a complex function which is frequency dependent and is given by the equation

$$B = B_0\,\{\tan^{-1}(\omega\theta) + (i/2)\ln(1 + \omega^2\theta^2)\}\,\omega^{-1} \quad \ldots\ldots (2)$$

where θ = the relaxation time of the charge cloud and B_0 = the frequency independent part of B. In equation 2

$$B_0 = (2\,\pi\,e^2\,q^2/\epsilon^2\,\mathbf{k}T)\,\Sigma\,n_j^{\infty}, \qquad (3)$$

where e = the charge on an electron, q = the charge per unit length of dislocation, n_j^{∞} = the concentration of the charged point defect of type j well away from the dislocation, ϵ = the dielectric constant, $\mathbf{k}$ = Boltzmann's constant, and T = the absolute temperature. From equation 3 it can be seen that B_0 is proportional to the total concentration of charged point defects and to the square of the charge on the dislocation.

TABLE I Summary of formulae for the orientation tensor α_{whr}.

	Edge Dislocation ($b_m\nu_m = 0$)
For σ_{11}	$\alpha_{w11} = (\nu_2 b_3 - \nu_3 b_2)b_1 b_w/b^3$
	$\alpha_{w11}\,\alpha_{w11} = (\nu_2 b_3 - \nu_3 b_2)^2\,b_1^2/b^4$
For σ_{12}	$\alpha_{w12} = \{\nu_3(b_1^2 - b_2^2) + b_3(\nu_2 b_2 - \nu_1 b_1)\}\,b_w/b^3$
	$\alpha_{w12}\,\alpha_{w12} = \{\nu_3(b_1^2 - b_2^2) + b_3(\nu_2 b_2 - \nu_1 b_1)\}^2/b^4$
	Screw Dislocation ($b_m = b\nu_m$)
For σ_{11}	$\alpha_{111} = 0$
	$\alpha_{211} = -\nu_1\nu_3$
	$\alpha_{311} = +\nu_1\nu_2$
	$\alpha_{w11}\,\alpha_{w11} = \nu_1^2(\nu_2^2 + \nu_3^2)$
For σ_{12}	$\alpha_{112} = \nu_1\nu_3$
	$\alpha_{212} = -\nu_2\nu_3$
	$\alpha_{312} = \nu_2^2 - \nu_1^2$
	$\alpha_{w12}\,\alpha_{w12} = \nu_3^2(\nu_1^2 + \nu_2^2) + (\nu_2^2 - \nu_1^2)^2$

Note – $b = (b_m b_m)^{\frac{1}{2}}$ and $\nu_m\nu_m = 1$.

$C\,(\partial^2\xi_w/\partial y^2)$ is the restoring force due to the curvature of the dislocation where

$$C \simeq G\,b^2/2\pi\,(1 - \nu),$$

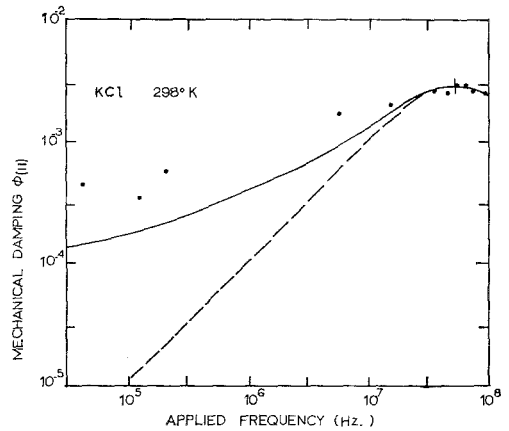

Figure 3 Mechanical Damping $\phi_{(11)}$ of KCl at 298°K, normalised to a dislocation density of 9.2×10^6 cm^{-2} ● from Suzuki *et al* [2] and ○ present paper. The solid line is the theoretical curve for charge cloud damping while the dashed line is for phonon damping.

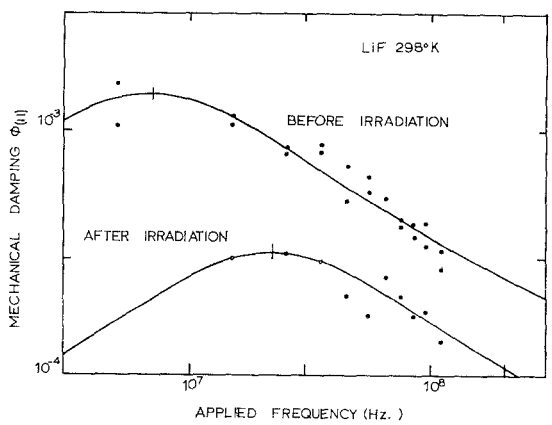

Figure 4 Mechanical Damping $\phi_{(11)}$ of LiF at 298°K before and after an X-ray irradiation of 10^3 Rontgen/cm^2 (from Suzuki *et al* [2]). The solid lines are theoretical curves for the charge cloud theory.

G is the shear modulus and ν is Poisson's ratio.

$\alpha_{wmn}\,b\sigma_{mn}\sin\omega t$ is the force per unit length due to the applied stress $\sigma_{mn}\sin\omega t$. The value for α_{wmn} the orientation tensor, is determined from the Peach-Koehler equation for the force acting on a dislocation by the stress system [12]. A summary of formulae for this tensor is contained in table I. In this table b_1, b_2, b_3 and ν_1, ν_2, ν_3 are the components of the Burgers vector and the normalised vector which defines the dislocation line.

2.1. Charge Cloud Damping

The differential equation (equation 1) can be solved for $\xi_w(y, t)$ by using a finite Fourier sine transform. The solution for $\xi_w(y, t)$ is

$$\xi_w(y, t) = \frac{4a_{wmn}\, b\sigma_{mn}}{\pi A} \sin \omega t \sum_{n=0}^{\infty} (2n + 1)^{-1} \left\{ \frac{\omega_n^2 - \omega^2 - (B_0/2A) \ln (1 + \omega^2\theta^2) - i (B_0/A) \tan^{-1} \omega\theta}{[\omega_n^2 - \omega^2 - (B_0/2A) \ln (1 + \omega^2\theta^2)]^2 + [(B_0/A) \tan^{-1} \omega\theta]^2} \right\} \sin[(2n + 1)\pi y/l] \quad (4)$$

where ω_n, the undamped resonant frequency for the dislocation loop, is given by

$$\omega_n = [(2n + 1)\pi/l]\,(C/A)^{\frac{1}{2}} \quad (5)$$

The mechanical damping ϕ can be obtained from this formula for $\xi_w(y, t)$ by computing the energy dissipated per unit volume in one cycle (ΔW) and dividing the answer by 2π times the total energy of vibration, W, where

$$W = S_{mnop}\, \sigma_{mn}\, \sigma_{op}/2 \quad (6)$$

S_{mnop} being the elastic compliance.* For a longitudinal wave, then

$$\phi_{(11)} = \frac{8}{\pi^2 A S_{1111}} \sum_s (a_{w11}\, a_{w11}\, b^2)_s \int_{l=0}^{\infty} N_s(l) \sum_{n=0}^{\infty} (2n + 1)^{-2} \left\{ \frac{(B_0/A) \tan^{-1} \omega\theta}{[\omega_n^2 - \omega^2 - (B_0/2A) \ln (1 + \omega^2\theta^2)]^2 + [(B_0/A) \tan^{-1} \omega\theta]^2} \right\} dl \quad (7)$$

while for a shear wave

$$\phi_{(12)} = \frac{8}{\pi^2 A S_{1212}} \sum_s (a_{w12}\, a_{w12}\, b^2)_s \int_{l=0}^{\infty} N_s(l) \sum_{n=0}^{\infty} (2n + 1)^{-2} \left\{ \frac{(B_0/A) \tan^{-1} (\omega\theta)}{\omega_n^2 - \omega^2 - (B_0/2A) \ln (1 \times \omega^2\theta^2)]^2 + [(B_0/A) \tan^{-1} \omega\theta]^2} \right\} dl \quad (8)$$

The compliance defect, $\Delta S_{\underline{hkhk}}/S_{\underline{hkhk}}$, is determined by calculating the dislocation strain $\Delta\epsilon_{hk}$ in-phase with the total strain and dividing the answer by the total strain (see equation 37, ref. 12). The compliance defects for the longitudinal wave and the shear wave are

As the order of the harmonic, $(2n + 1)$, increases the mechanical damping and the compliance defect decrease at a rate governed by $(2n + 1)^{-2}$ so that their values for $n = 1$ are only one ninth of those for $n = 0$. This means that only the first harmonic, $n = 0$, needs to be considered. Since the distribution of loop lengths $N_s(l)$ is unknown in this paper it will be assumed that all the dislocations are of the same loop length, that is, the distribution of loop lengths is a delta function.

In the high temperature experiments of Robinson and Birnbaum it was found that the charge cloud was almost stationary ($\omega\theta > 1$) and that $[(B_0/A) \ln (\omega\theta)]^{\frac{1}{2}}$ is far greater than the radial frequency of the applied stress ($(B_0/A) \ln (\omega\theta) > \omega^2$).

Using the above three assumptions then if only one slip system is operative the equations for the mechanical damping and compliance defect become

$$(\Delta S_{1111}/S_{1111}) = \frac{8}{\pi^2 A S_{1111}} \sum_s (a_{w11}\, a_{w11}\, b^2)_s \int_{l=0}^{\infty} N_s(l) \sum_{n=0}^{\infty} (2n + 1)^{-2} \left\{ \frac{\omega_n^2 - \omega^2 - (B_0/2A) \ln (1 + \omega^2\theta^2)}{[\omega_n^2 - \omega^2 - (B_0/2A) \ln (1 + \omega^2\theta^2)]^2 + [(B_0/A) \tan^{-1} \omega\theta]^2} \right\} dl \quad (9)$$

and

$$(\Delta S_{1212}/S_{1212}) = \frac{8}{\pi^2 A S_{1212}} \sum_s (a_{w12}\, a_{w12}\, b^2)_s \int_{l=0}^{\infty} N_s(l) \sum_{n=0}^{\infty} (2n + 1)^{-2} \left\{ \frac{\omega_n^2 - \omega^2 - (B_0/2A) \ln (1 + \omega^2\theta^2)}{[\omega_n^2 - \omega^2 - (B_0/2A) \ln (1 + \omega^2\theta^2)]^2 + [(B_0/A) \tan^{-1} \omega\theta]^2} \right\} dl \quad (10)$$

*For the pulse echo technique a displacement rather than a stress is specified for the crystal so that $W = C^{-1}{}_{mnop}\, \epsilon_{mn}\epsilon_{op}/2$ and the compliance in equations 7 and 8 should then be replaced by the inverse of the stiffness.

$$\phi(\underline{hk}) = \frac{8}{\pi^2 A S_{\underline{hkhk}}} (a_{w\underline{hk}} a_{w\underline{hk}})_s b^2(N_s l) \left\{ \frac{(B_0/A)\,\pi/2}{[\omega_0^2 - (B_0/A)\ln\omega\theta]^2 + [(B_0/A)\,\pi/2]^2} \right\} \quad (11)$$

and

$$(\Delta S_{\underline{hkhk}}/S_{\underline{hkhk}}) = \frac{8}{\pi^2 A S_{\underline{hkhk}}} (a_{w\underline{hk}}\, a_{w\underline{hk}})_s\, b^2(N_s l) \left\{ \frac{\omega_0^2 - (B_0/A)\ln\omega\theta}{[\omega_0^2 - (B_0/A)\ln\omega\theta]^2 + [(B_0/A)\,\pi/2]^2} \right\} \quad (12)$$

Now $\phi_{(\underline{hk})}$ has a maximum of

$$\phi_{(\underline{hk})}(\max) = 16(a_{w\underline{hk}}\, a_{w\underline{hk}})_s\, b^2(N_s l)/(\pi^3 B_0 S_{\underline{hkhk}}) \quad \ldots\ldots (13)$$

when

$$\omega = \omega(\max) = \theta^{-1} \exp(\omega_0^2 A/B_0). \quad (14)$$

Equations 11 and 12 can be readily normalised giving

$$\phi_{(\underline{hk})}/\phi_{(\underline{hk})}(\max) = \{4\,[\ln(\omega/\omega(\max))]^2/\pi^2 + 1\}^{-1} \quad \ldots\ldots (15)$$

and

$$(\Delta S_{\underline{hkhk}}/S_{\underline{hkhk}})/(\Delta S_{\underline{hkhk}}/S_{\underline{hkhk}})(\max) = -4\ln(\omega/\omega(\max))/\{4\,[\ln(\omega/\omega(\max))]^2/\pi^2 + 1\}\,\pi \quad \ldots\ldots (16)$$

where

$$(\Delta S_{\underline{hkhk}}/S_{\underline{hkhk}})(\max) = (a_{w\underline{hk}}\, a_{w\underline{hk}})_s\, b^2(N_s l)/(\pi^3 B S_{\underline{hkhk}}) = \phi(\underline{hk})(\max)/2 \quad \ldots\ldots (17)$$

when $\ln(\omega/\omega(\max)) = -\pi/2$.

These two normalised equations are plotted in figs. 1 and 2. Fig. 1 shows the relatively slow change of $\phi_{(\underline{hk})}$ with frequency. It is interesting to note that it is possible to normalise these equations so that the shapes of these curves are not dependent on the relative magnitudes of the parameters ω_0, B_0/A and $\omega\theta$ though, of course, at very high frequencies when $\omega \sim \omega_0$ it is no longer possible to carry out the normalisation process and this is no longer true.

From equations 3 and 13 it can be seen that $\phi_{(\underline{hk})}(\max)$ is inversely proportional to the concentration of charged point defects and the square of the charge on the dislocation and is not affected by dislocation pinning as long as the total length of dislocation loops, $N_s l$, on each slip plane remains unchanged. The radial frequency at which the maximum in damping occurs (equation 14) is through the expotential very strongly dependent on the loop length l ($\omega_0 \propto l^{-1}$), the defect concentration and the charge on the dislocation ($B_0 \propto q^2 \sum n_j^{\infty}$).

2.2. Phonon Damping

For phonon damping where B is not frequency dependent then the displacement

$$\xi_w(y, t) = \frac{4\alpha_{wmn}}{\pi A} b\sigma_{mn} \sin\omega t \sum_{n=0}^{\infty} (2n+1)^{-1} \left\{ \frac{\omega_n^2 - \omega^2 - i\omega B/A}{[\omega_n^2 - \omega^2]^2 + (B/A)^2\omega^2} \right\} \sin\frac{(2n+1)\pi y}{l} \quad (18)$$

and the damping and compliance defect due to N_s dislocations of loop length l is

$$\phi_{(\underline{hk})} = \frac{8}{\pi^2 A S_{\underline{hkhk}}} (a_{w\underline{hk}}\, a_{w\underline{hk}})_s\, b^2(N_s l) \left\{ \frac{\omega B/A}{[\omega_0^2 - \omega^2]^2 + (B/A)^2\omega^2} \right\} \quad (19)$$

and

$$\Delta S_{\underline{hkhk}}/S_{\underline{hkhk}} = \frac{8}{\pi^2 A S_{\underline{hkhk}}} (a_{w\underline{hk}}\, a_{w\underline{hk}})_s\, b^2(N_s l) \left\{ \frac{\omega_0^2 - \omega^2}{[\omega_0^2 - \omega^2]^2 + (B/A)^2\omega^2} \right\} \quad (20)$$

Where dislocations are overdamped ($\omega_0 > \omega$) then

$$\phi_{(\underline{hk})} = \frac{8}{\pi^2 A S_{\underline{hkhk}}} (a_{w\underline{hk}}\, a_{w\underline{hk}})_s\, b^2(N_s l) \left\{ \frac{\omega B/A}{\omega_0^4 + \omega^2 B^2/A^2} \right\} \quad (21)$$

and

$$\Delta S_{\underline{hkhk}}/S_{\underline{hkhk}} = \frac{8}{\pi^2 A S_{\underline{hkhk}}} (a_{w\underline{hk}}\, a_{w\underline{hk}})_s\, b^2(N_s l) \left\{ \frac{\omega_0^2}{\omega_0^4 + \omega^2 B^2/A^2} \right\} \quad (22)$$

$\phi_{(\underline{hk})}$ has a maximum of

$$\phi_{(\underline{hk})}(\max) = \frac{4}{\pi^2 B S_{\underline{hkhk}}} \frac{(a_{w\underline{hk}}\, a_{w\underline{hk}})_s\, b^2(N_s l)}{\omega(\max)} \quad (23)$$

at

$$\omega = \omega(\max) = \omega_0^2 A/B \quad (24)$$

while

$$\phi_{(\underline{hk})}(\max)\,\omega(\max) = \frac{4(a_{w\underline{hk}}\, a_{w\underline{hk}})_s}{\pi^2 S_{\underline{hkhk}} B} b^2 (N_s l) \quad (25)$$

The equations for $\phi_{(\underline{hk})}$ and $\Delta S_{\underline{hkhk}}/S_{\underline{hkhk}}$ may be readily normalised giving

$$\phi_{(\underline{hk})}/\phi_{(\underline{hk})}(\max) = 2(\omega/\omega(\max))/[1 + (\omega/\omega(\max))^2] \quad (26)$$

and

$$(\Delta S_{\underline{hkhk}}/S_{\underline{hkhk}})/(\Delta S_{\underline{hkhk}}/S_{\underline{hkhk}})(\max) = [1 + (\omega/\omega(\max))^2]^{-1}. \quad (27)$$

These two equations have the same form as the formuli for a Debye relaxation and are shown in figs. 1 and 2.

From these figures the difference in shape of the curves for the two theories for amplitude independent damping can readily be seen. At very low frequencies $\phi_{(hk)}$ for the G-L theory is proportional to ω while for the R-B theory the damping varies as $[\ln(\omega/\omega(\max))]^{-2}$. The compliance defect in the G-L theory decreases smoothly from a maximum at low frequencies to a minimum at high frequencies with most of the change occurring near $\omega(\max)$. In the R-B theory the compliance defect is small at low frequencies, increases slowly to a maximum at $\ln(\omega/\omega(\max)) = -\pi/2$, decreases rapidly to zero at $\omega = \omega(\max)$ before going to a minimum at $\ln(\omega/\omega(\max)) = \pi/2$ and approaching zero at higher frequencies.

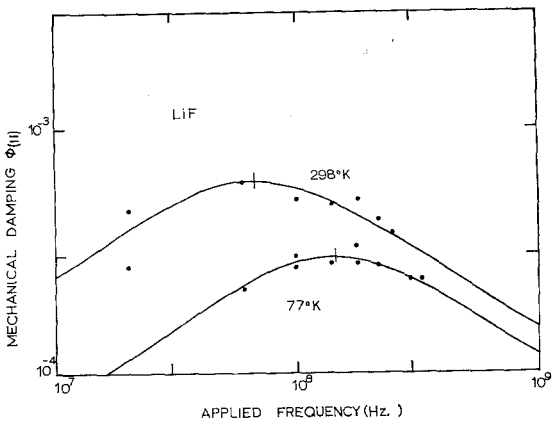

Figure 5 Mechanical Damping $\phi_{(11)}$ of LiF at 298 and 77°K (from Mitchell [1]). The solid lines are theoretical curves for the charge cloud theory.

3. Experimental Procedure and Results

In this paper experimental results from three sources will be discussed. First the published work of Suzuki *et al* [2], on LiF and KCl in the frequency range of 5 to 100 MHz will be presented, then the results of Mitchell [1] on LiF at frequencies of 20 to 500 MHz and lastly some recent results of the author on KCl at 40, 120 and 200 kHz.

In 1964 Suzuki, Ikushima, and Aoki published the results of a series of damping experiments which they had carried out at room temperature on single crystals of LiF and KCl in the frequency range of 5 to 100 MHz [2]. In their experiments they measured the decay of an ultrasonic signal generated by a 5 MHz quartz transducer when this signal was passed through specimens of about 1 × 1 × 1 cm. Some of their results, for KCl and LiF specimens which had been plastically deformed and then annealed (dislocation density $\sim 10^7$ cm^{-2}), are shown in figs. 3 and 4 together with the results of an X-ray irradiation of 10^3 Rontgen/cm^2 (density of F-centres $\sim 10^{16}$ cm^{-3} or $\sim 10^{-7}$) on the LiF specimen. These results show that the damping has a maximum at $\sim$ 10 MHz ($\omega(\max) \sim 10^8$ radians/sec) and that on irradiation the size of this maximum is reduced and moves to a higher frequency.

In her 1965 paper, Mitchell presents some results for the attenuation of ultrasonic longitudinal and shear waves along a ⟨100⟩ direction. In this experiment the attenuation was measured by a conventional pulse-echo technique in the 10 to 400 MHz range before and after a slight plastic compression (0.05 to 0.1%). At room temperature 10 and 20 MHz quartz transducers were used while at 77 and 20K a 10 MHz crystal was found to be satisfactory. The increase in attenuation observed for longitudinal waves was attributed to dislocations generated during the deformation while the lack of increase in attenuation for shear waves was not surprising since the force on dislocations in this case is zero.

The mechanical damping versus frequency for a LiF crystal at 77 and 298°K is shown in fig. 5. The damping has a maximum at $\sim$ 100 MHz ($\omega(\max) \sim 10^9$ sec^{-1}) and on going from 298 to 77°K this maximum decreases and occurs at a higher frequency.

The 40, 120 and 200 kHz points shown in fig. 3 are the damping values for a ⟨100⟩ KCl specimen measured on a composite oscillator vibrating in the longitudinal mode at room temperature with a strain amplitude of $\sim 10^{-7}$ (amplitude-independent region). The specimen was measured in the as-received state from Harshaw Chemical Co and has a dislocation density of $\sim 3 \times 10^6$ cm^{-2}. This dislocation density was determined by etching the crystals in a 25% concentrated solution of $BaBr_2$ in methyl alcohol and counting the etch pits. The results plotted in fig. 3 have been normalised to the dislocation density of 9.2×10^6 cm^{-2} reported for the high frequency results of Suzuki *et al*. As can be seen from fig. 3 the results for

TABLE II Summary of experimental results

	ϕ(max)	ω(max) $r\ sec^{-1}$	$(N_s l)$ cm^{-2}	R-B theory				G-L theory
				B_0 mks from equation 13	$\sum n_j^{\infty}$	q C-m^{-1} from equation 3	q/q(max)	B mks from equation 25
KCl (298°K)	3×10^{-3}	3.2×10^{8}	9.2×10^{6}	3.0×10^{4}	10^{-5}	3.1×10^{-12}	1.2%	7.4×10^{-5}
LiF (298°K before irrad.)	1.4×10^{-3}	4.4×10^{7}	2.8×10^{6}	2.3×10^{4}	10^{-5}	1.4×10^{-12}	0.35%	4.2×10^{-4}
LiF (298°K after irrad.)	3.2×10^{-4}	1.4×10^{8}	2.8×10^{6}	1.0×10^{5}	if 10^{-5}	then 2.9×10^{-12}	0.73%	5.8×10^{-4}
					if 4.3×10^{-5}	then 1.4×10^{-12}	0.35%	
LiF (298°K)	6×10^{-4}	4.1×10^{8}	8×10^{5}	1.6×10^{4}	10^{-5}	1.1×10^{-12}	0.29%	3.0×10^{-5}
LiF (77°K)	3×10^{-4}	9.1×10^{8}	8×10^{5}	3.1×10^{4}	if 10^{-5}	then 8.1×10^{-13}	0.20%	2.7×10^{-5}
					if 5.1×10^{-6}	then 1.1×10^{-12}	0.29%	
					if 1.3×10^{-6}	then 2.2×10^{-12}	0.58%	

Note – B_0 mks $= 10B_0$(cgs) and B(mks) $= 10B$(cgs).

damping at kHz frequencies are lower than those at MHz frequencies.

4. Discussion

4.1. KCl Results

The solid line in fig. 3 is a plot of equation 15 (R-B theory) while the dotted line is a plot of equation 26 from the theory of Granato and Lücke. As can be seen in this figure the theoretical R-B curve of $\phi_{(11)}$ fits the experimental points better than the G-L curve which is far too steep to include the kHz damping results. The relevant results for $\phi_{.11.}$ (max), w (max), dislocation density, B_0, q, and B for the two theories is summarised in table II.

If reasonable values are chosen for the parameters S_{1111}, b and $N_s l$ ($S_{1111} = 25.9 \times 10^{-12}$ m²/N, $b = 4.45$Å and $N_s l = 9.2 \times 10^{10}$m/m³) then by substituting the experimental value for $\phi_{(11)}$(max) in equation 13 one obtains $B_0 = 9.5 \times 10^4$ N/m². For a total divalent impurity concentration, $\sum n_j^{\infty}$, of the order of 10^{-5} (10 ppm), then from equation 3 q becomes 3.1×10^{-12} C/m which means that the dislocation is carrying 1.2% of its saturation value. This figure for the charge on the dislocation compares very favourably with the results of q/q(max) ~ 1 to 3% obtained for potassium chloride by Robinson using a piezoelectric technique [12]. It should be noted that $A \sim 10^{-15}$ kg/m so that $B_0/A \sim 10^{20}$ sec^{-2} while $\omega^2 \sim 10^{18}$ sec^{-2} confirming the approximation $(B_0/A) \ln \omega\theta > \omega^2$ used to obtain equation 11. For a dislocation loop length of 10^3Å (10^{-7} m) then ω_0, the resonant frequency of the undamped dislocation, is 4×10^{10} sec^{-1} giving $\omega_0^2 \sim 2 \times 10^{21}$ sec^{-2} which means that $\omega_0^2 \sim (B_0/A) \ln \omega\theta$.

4.2. Effect of Irradiation on LiF

The results of Suzuki *et al* before and after irradiation are plotted in fig. 4, the solid lines being the theoretical curves of the R-B theory (equation 13). The values for the various parameters are contained in table II.

The results for the LiF specimen before irradiation are similar to those of the KCl specimen giving about the same values of B_0 and q while B is 5.7 times that of KCl. The effect of the relatively light X-ray irradiation is very interesting in that it causes both a decrease in $\phi_{(11)}$(max) and an increase in ω(max). Using the theory of Granato and Lücke it is possible to explain both these changes as being due to an increase in the number of dislocation pinning points causing ω_0 to rise. On irradiation the value of B increases by 37%, a change which is difficult to explain in terms of phonon damping though the values are as close as can be expected considering the scatter of the experimental results and they are consistent with the loop length of the dislocations being halved on irradiation.

Comparing the results of irradiation with the theory of R-B it is found that the results before irradiation of LiF give about the same values for B_0 and q as the KCl specimen (table II). The effect of the relatively light X-ray irradiation is to increase B_0 by a factor of 4.5. This is very interesting in that if the irradiation increased B_0 without affecting ω_0, then one would expect ω(max), because of its exponential dependence on B_0 (equation 14), to change from $\sim 5 \times 10^7$ sec^{-1} to $\sim 5 \times 10^{35}$ sec^{-1}. However, ω(max) increases only slightly so that to a first approximation it can be said that ω(max) remains constant hence the mean loop length must decrease to about one half of its non-irradiated value while B_0 increases five-fold. This five-fold increase in B_0 may be due either to a five-fold increase in the total concentration of charged defects ($\sum n_j^{\infty}$) or to an increase by a factor of two in the charge on the dislocation (see equation 3 and table II). Since before irradiation $\sum n_j^{\infty} \sim 10^{-5}$ and after the low X-ray irradiation of 10^3 Rontgen/cm² the F-centre concentration is $\sim 10^{-7}$, it is extremely unlikely that the effect of irradiation is a five-fold increase in $\sum n_j^{\infty}$. Instead the effect of the irradiation is expected to be a doubling of both the dislocation pinning and the dislocation charge.

4.3. Effect of Temperature on LiF

The results shown in fig. 5 are from the paper of Mitchell and the analysed data is tabulated in table II. On decreasing the temperature the frequency at which maximum damping occurs increases while the magnitude of the maximum decreases.

In terms of the theory of Granato and Lücke the effect of decreasing the temperature from 298 to 77 K is to decrease the damping constant B by 11% while the mean dislocation loop length is decreased by 33%. Both these results are reasonable. The value of B for these specimens is $\frac{1}{14}$ of that obtained for Suzuki *et al* LiF. This large difference is difficult to understand since one would not expect the phonon damping to vary greatly from one specimen to another even if the impurity level did change.

When compared with the theory of Robinson and Birnbaum the effect of temperature suggests that on decreasing the temperature from 298 to 77 K B_0 is doubled while the loop length is decreased by 40%. The doubling of B_0 is in part due to decreasing the temperature by a factor of four. Because of the relatively small change in ω(max) it is concluded that the doubling of B_0 is accompanied by a 40% decrease in the mean dislocation loop length. The charge on the dislocation on cooling is expected to increase by 40% while due to precipitation the total concentration of charged defects ($\sum n_j^{\infty}$) is halved. It is important to note that at room temperature the charge on the dislocations for the Mitchell and unirradiated Suzuki *et al* LiF specimens is 0.35% and 0.29% of saturation, a result which gives support to the theory of charge cloud damping

5. Conclusions

All the damping results presented in this paper have been shown to be consistent with the theory of damping due to charged dislocations oscillating within their practically immobile ($\omega\theta > 1$) charge clouds. The calculated results of q/q(max) $\sim$ 0.2 to 1.2% for the charge on the dislocations are reasonable and are in agreement with the results of more direct measurements. The increase in B_0 due to irradiation can be explained by an increase in either the concentration of charged defects or charge on the dislocation. From the change in B_0 and the small change in ω(max) it is concluded that most likely both the dislocation pinning and dislocation charge are doubled by the X-ray irradiation while there is little change in the concentration of charge defects well away from the dislocation. The conclusion suggests that defects are more easily formed at the dislocations than in the rest of the solid. The results for a decrease in temperature from 298 to 77 K are consistent with a 40% increase in the charge on the dislocation together with a 40% decrease in the mean dislocation loop length and 75% of the total charged point defects being precipitated out. The close agreement of the values of the charge on the dislocations for the LiF specimens of Mitchell and Suzuki *et al* confirm the charge cloud damping theory.

For the phonon damping theory the kHz damping results are too high when compared with the results in the MHz region. The effect of irradiation in terms of this theory is to decrease the mean loop length to one half of its original value while decreasing the temperature from 298 to 77 K causes the damping constant B to decrease by 11% and the dislocation loop length to drop by $\sim$ 40%. The damping constant for the Suzuki *et al* specimen is found to be fourteen times that for Mitchells suggesting that the phonon damping theory is not applicable to alkali halides at least not in its present form with a frequency independent damping constant.

The damping experiments discussed in this paper indicate that in alkali halides the motion of dislocations is damped by the interaction with surrounding charge clouds. To distinguish more clearly between phonon damping and charge cloud damping it is necessary to measure the charge on the dislocation when the specimen is irradiated or its temperature is changed. This may be done by measuring the piezoelectric effect and mechanical damping [12]. Since the compliance defect as a function of frequency is quite different for the two forms of damping then another worthwhile experiment would be measuring the mechanical damping and compliance defect over a range of frequencies.

References

1. O. M. MRACEK MITCHELL, *J. Appl. Phys.* **35** (1965) 2083.
2. T. SUZUKI, A. IKUSHIMA, and M. AOKI, *Acta Metallurgica* **12** (1964) 1231.
3. W. H. ROBINSON and H. K. BIRNBAUM, *J. Appl. Phys.* **37** (1966) 3754.
4. K. L. KLIEWER and J. S. KOEHLER, *Phys. Rev. A.* **157** (1967) 685.
5. A. GRANATO and K. LÜCKE, *J. Appl. Phys.* **27** (1956) 583, 789.
6. G. LEIBFRIED, *Z. Physik* **127** (1950) 344.
7. W. P. MASON, *J. Acoust. Soc. Amer.* **32** (1960) 458.
8. G. A. BIELIG and H. F. POLLARD, IPPS Conference on the Science of Materials, New Zealand DSIR (1969) 104.
9. J. D. ESHELBY, C. W. A. NEWEY, and P. L. PRATT, *Phil. Mag.* **3** (1958) 75.
10. W. H. ROBINSON, IPPS Conference on the Science of Materials, New Zealand DSIR (1969) 113.
11. L. M. BROWN, *Phys. Stat. Sol.* **1** (1961) 585.
12. W. H. ROBINSON, New Zealand Physics and Engineering Lab, Tech. Note 219 (1970).

Received 15 March and accepted 20 August 1971.